Activation of Nitroarenes in the Homogenous Catalytic Carbonylation of Nitroaromatics via an Oxygen-Atom-Transfer Mechanism Induced by Inner-Sphere Electron Transfer†

Steven J. Skoog and Wayne L. Gladfelter*

Contribution from the Department of Chemistry, University of Minnesota, Minneapolis, Minnesota 55455

Received June 9, 1997⊗

Abstract: Kinetic and mechanistic studies on the deoxygenation of nitroarenes by Ru(dppe)$(CO)_3$, where dppe = 1,2-bis(diphenylphosphino)ethane, are described. The products of the reaction included 1 equiv of carbon dioxide and an η^2-nitrosoarene ruthenium complex (Ru(dppe)$(CO)_2$[ON(Ar)] for Ar = 4-chloro-2-trifluoromethylphenyl), which was isolated and fully characterized by solution spectroscopic methods and by single crystal X-ray diffraction [monoclinic crystal system, space group $P2_1/c$ (#14), a = 14.556 (8) Å, b = 12.903 (6) Å, c = 20.10 (1) Å, β = 105.60 (6)°, V = 3636 (8) Å^3, Z = 4]. The deoxygenation reaction was determined to be first-order with respect to both Ru(dppe)$(CO)_3$ and nitroarene. Electron withdrawing substituents on the nitroarene and polar solvents accelerated the rate, and a substituent study provided a ρ of +3.45 indicating negative charge buildup on the nitroarene in the rate determining step of the reaction. Activation enthalpies for 2-CF_3, 4-Cl, 4-H, and 4-CH_3 substituted nitroarenes were 9.3, 9.9, 10.5, and 10.7 kcal mol^{-1}, and the entropies of activation were −35, −33, −36, and −37 eu, respectively. Correlation between the reduction potentials of the nitroarenes ($E°_{ArNO2}$) and log k_2 was also observed for substituted nitroarenes yielding a slope of 10 V^{-1}. Monosubstituted nitroarenes bearing a single methyl, phenyl, or chloro group in the ortho position and disubstituted 2,6-dimethyl- and 2,3-dichloronitrobenzene showed no attenuation in the rate, from what would be expected based on the $E°_{ArNO2}$ − log k_2 correlation. Large rate attenuation was observed for nitroarenes bearing both ortho and meta groups. Analysis of the kinetic and thermodynamic data using Marcus theory indicated that the rates were too high for an outer-sphere electron-transfer mechanism. The data were interpreted in terms of an inner-sphere electron-transfer mechanism where the unfavorable energetics are mitigated by bonding interactions between the donor and acceptor.

Introduction

The homogeneous catalytic carbonylation of nitroaromatics shown in eq 1[1] provides

$$ArNO_2 + 3CO + MeOH \rightarrow ArNHC(O)OMe + 2CO_2 \quad (1)$$

one promising phosgene-free method for the production of aryl carbamates. A variety of ruthenium,[2−12] rhodium,[12−14] and palladium[15−20] complexes catalyze this reaction. In previous work with the catalyst system Ru(dppe)$(CO)_3$ (**1**), where dppe is 1,2-bis(diphenylphosphino)ethane, the catalyst **1** was shown to react with nitroarenes in the presence of carbon monoxide to form the metallacycle shown in eq 2 along with 1 equiv of carbon dioxide.[8]

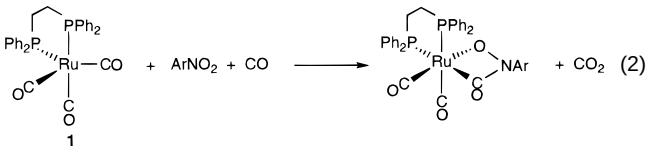

(2)

We undertook the current study to elucidate the mechanism of this reaction. Work of Berman and Kochi[21] on the deoxygenation of nitroarenes by nickel phosphine complexes (eq 3)

† Homogenous Catalytic Carbonylation of Nitroaromatics. 10. For part 9, see ref 22.

⊗ Abstract published in *Advance ACS Abstracts,* October 15, 1997.

(1) Cenini, S.; Pizzotti, M.; Crotti, C. In *Aspects of Homogeneous Catalysis*; Ugo, R., Ed.; Reidel: Dordrecht, 1988; Vol. 6, pp 97−198.

(2) Bhaduri, S.; Sharma, K. R.; Khwaja, H. I. *Proc. Indian Acad. Sci., Chem. Sci.* **1989**, *101*, 195.

(3) Cenini, S.; Pizzotti, M.; Crotti, C.; Porta, F.; La Monica, G. *J. Chem. Soc., Chem. Commun.* **1984**, 1286.

(4) Cenini, S.; Crotti, C.; Pizzotti, M.; Porta, F. *J. Org. Chem.* **1988**, *53*, 1243.

(5) Cenini, S.; Pizzotti, M.; Crotti, C.; Ragaini, F.; Porta, F. *J. Mol. Catal.* **1988**, *49*, 59.

(6) Gargulak, J. D.; Noirot, M. D.; Gladfelter, W. L. *J. Am. Chem. Soc.* **1991**, *113*, 1054.

(7) Gargulak, J. D.; Hoffman, R. D.; Gladfelter, W. L. *J. Mol. Catal.* **1991**, *68*, 289.

(8) Gargulak, J. D.; Berry, A. J.; Noirot, M. D.; Gladfelter, W. L. *J. Am. Chem. Soc.* **1992**, *114*, 8933.

(9) Gargulak, J. D.; Gladfelter, W. L. *Inorg. Chem.* **1994**, *33*, 253.

(10) Grate, J. H.; Hamm, D. R.; Valentine, D. H. U.S. Patent 4603216, 1986.

(11) Grate, J. H.; Hamm, D. R.; Valentine, D. H. U.S. Patent 4629804, 1986.

(12) Grate, J. H.; Hamm, D. R.; Valentine, D. H. U.S. Patent 4705883, 1987.

(13) Ragaini, F.; Cenini, S.; Demartin, F. *J. Chem. Soc., Chem. Commun.* **1992**, 1467.

(14) Ragaini, F.; Cenini, S.; Demartin, F. *Organometallics* **1994**, *13*, 1178.

(15) Braunstein, P.; Bender, R.; Kervennal, J. *Oganometallics* **1982**, *1*, 1236.

(16) Ugo, R.; Psaro, R.; Pizzotti, M.; Nardi, P.; Dossi, C.; Andreetta, A.; Capparella, G. *J. Organomet. Chem.* **1991**, *417*, 211.

(17) Valli, V. L. K.; Alper, H. *J. Am. Chem. Soc.* **1993**, *115*, 3778.

(18) Leconte, P.; Metz, F.; Mortreux, A.; Osborn, J. A.; Paul, F.; Petit, F.; Pillot, A. *J. Chem. Soc., Chem. Commun.* **1990**, 1616.

(19) Cenini, S.; Ragaini, F.; Pizzotti, M.; Porta, F.; Mestroni, G.; Alessio, E. *J. Mol. Catal.* **1991**, *64*, 179.

(20) Wehman, P.; Dol, G. C.; Moorman, E. R.; Kramer, P. C. J.; van Leeuwen, P. W. N. M.; Fraanje, F.; Goubitz, K. *Organometallics* **1994**, *13*, 4856.

(21) Berman, R. S.; Kochi, J. K. *Inorg. Chem.* **1980**, *19*, 248.

S0002-7863(97)01899-4 CCC: $14.00

$$Ni(PR_3)_4 + R'NO_2 \rightarrow Ni(PR_3)_2(R'NO) + PR_3 + PR_3O \quad (3)$$

provided kinetic evidence for a single-electron transfer pathway and suggested that a side-bound nitrosoarene nickel complex was formed. Side-bound nitrosoarene complexes have been previously isolated and characterized in mono-metallic complexes[22−26] and in metal clusters.[27−31] These complexes have been suggested to be important intermediates in the homogeneous catalytic carbonylation of nitroaromatics.[1] In the current study we provide kinetic evidence that the initial deoxygenation proceeds via rate-determining inner-sphere electron transfer. In addition, we isolated an intermediate η^2-nitrosoarene ruthenium complex **2** as the product (eq 4). Marcus theory was used to

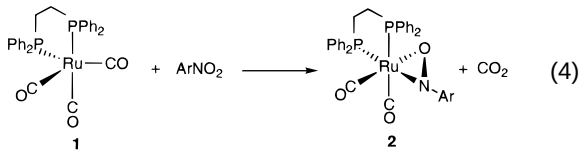

(4)

assess the energetic factors governing the electron transfer.[32−34]

Experimental Section

General. Standard Schlenk techniques were used in handling all organometallic compounds.[35] A nitrogen-filled Vacuum Atmospheres dry box equipped with a Dri-Train Model 40-1 inert gas purifier or a MBraun 150-M dry box were used for manipulations requiring inert atmosphere conditions. The compounds 1,2-bis(diphenylphosphino)-ethane and $Ru_3(CO)_{12}$ were purchased from Strem chemicals; the former was purified by recrystallization from hexane/toluene. Nitroarenes were purchased from commercial sources. Solid nitroarenes were either recrystallized from hexane/toluene or sublimed; liquid nitroarenes were extracted with hydrochloric acid and sodium hydroxide, dried over magnesium sulfate, vacuum distilled from phosphorous pentoxide or calcium hydride, and stored under nitrogen over 4 Å molecular sieves. $Ru(dppe)(CO)_3$,[36] $[Ru_2(dppe)_2(CO)_6](PF_6)_2$,[37] arylazoxy,[38] arylazo,[39] dinitrodurene,[40] and 2,4,6-triisopropyltrinitrobenzene[41] compounds were prepared according to literature procedures. Carbon monoxide (CP grade) was used for all reactions carried out under a CO atmosphere.

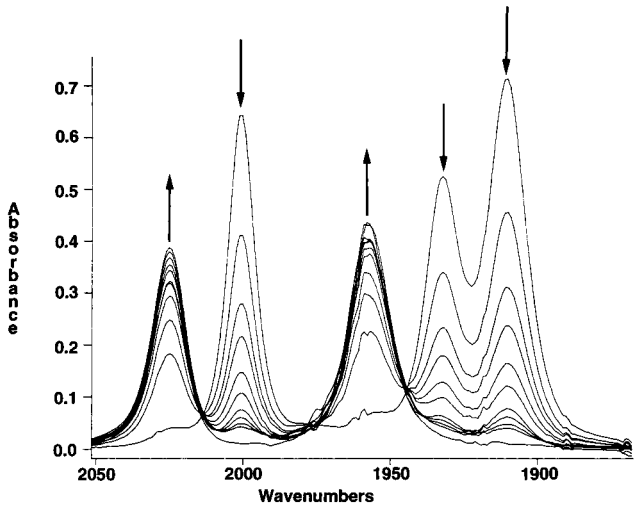

Figure 1. Infrared spectra in the ν_{CO} region of the progress of the reaction between $Ru(dppe)(CO)_3$ (**1**) and 2-trifluoromethylnitrobenzene in THF at 25 °C. Peaks at 1910, 1932, and 2001 cm^{-1} correspond to **1**, and peaks at 1957 and 2025 cm^{-1} correspond to $Ru(dppe)(CO)_2[ON(2\text{-}CF_3C_6H_4)]$ (**2c**).

Solvents were distilled prior to use under prepurified nitrogen; THF, toluene, and hexane were distilled from sodium benzophenone ketyl; methylene chloride and deuterated methylene chloride were distilled from calcium hydride and stored under nitrogen over 4 Å molecular sieves. All infrared spectral measurements were carried out on a Mattson Polaris FTIR spectrometer. The ^1H, $^{13}C\{^1H\}$, ^{19}F, and $^{31}P\{^1H\}$ NMR spectral studies were performed using a Varian Unity 300 MHz spectrometer. Proton and $^{13}C\{^1H\}$ NMR spectra were referenced to resonances corresponding to residual protons or carbon atoms of the solvent. ^{19}F NMR spectra were externally referenced to CCl_3F (δ = 0.0 ppm), and $^{31}P\{^1H\}$ NMR spectra were externally referenced to 85% H_3PO_4 (δ = 0.0 ppm). Electronic absorption spectra were obtained on a HP 8452A diode array spectrometer. The ionspray (IS) mass spectrometric experiments employed a triple quadrupole mass spectrometer (API III LC-MS-MS system, Sciex, Thornhill, Ontario, Canada), and FAB mass spectrometric experiments were obtained on a VG 7070E-HF instrument. Gas chromatography was performed on an HP 5890 series II using a 10 m megabor FFAP cross-linked column with a flame ionizing detector. Microanalyses were carried out by M-H-W laboratories.

Kinetic Studies. The reactions between **1** and nitroarenes in THF were studied by following the decrease of the carbonyl stretch at 2001 cm^{-1} corresponding to **1**. A representative set of spectral changes is shown in Figure 1, where the nitroarene was 2-(trifluoromethyl)nitrobenzene. The peak at 1909 cm^{-1} was followed in experiments using solvents other than THF and in experiments carried out under an atmosphere of CO. The reaction flasks, equipped with Teflon-coated stir bars and serum-capped gas adapters, were charged with **1** in a glovebox. The nitroarenes were added to the volumetric flask either via syringe under an inert atmosphere for liquids, or transferred as a solid in a glovebox; the solvent was then added, and the solution was transferred to a Schlenk tube for degassing using three freeze−pump−thaw cycles. After the final degassing cycle, the temperature of the solution was equilibrated to the reaction temperature held constant to ±0.1 °C using a Haake A81 constant temperature controller. At appropriate time intervals small aliquots were withdrawn from the reaction flasks via syringe and quickly analyzed in the FTIR spectrometer. For reactions that had half-lives shorter than several hours, the aliquots were transferred to small nitrogen-purged, serum-capped vials, frozen at −198 °C, thawed to −78 °C, and rapidly scanned in the spectrometer. This procedure was not possible when using anhydrous DMSO (Aldrich) as the solvent even though the half-life was less than 1 h. The concentration of nitroarene was at least 10-fold greater than that of **1**, and the pseudo-first-order rates were obtained by plotting ln ($A_t - A_\infty$) vs time as seen in Figure 2. Reactions having half-lives longer than 24 h A_∞ values were estimated from previous runs. Each kinetic experiment was run at least in triplicate, and the

(22) Skoog, S. J.; Campbell, J. P.; Gladfelter, W. L. *Organometallics* **1994**, *13*, 4137.
(23) Liebeskind, L. S.; Sharpless, K. B.; Wilson, R. D.; Ibers, J. A. *J. Am. Chem. Soc.* **1978**, *100*, 7061.
(24) Pizzotti, M.; Porta, F.; Cenini, S.; Demartin, F.; Masciocchi, N. *J. Organomet. Chem.* **1987**, *330*, 265.
(25) Brouwer, E. B.; Ledzdins, P.; Rettig, S. J.; Ross, K. J. *Organometallics* **1994**, *13*, 2088.
(26) Ridouane, F.; Sanchez, J.; Arzoumanian, H.; Pierrot, M. *Acta Crystallogr.* **1990**, *C46*, 1407.
(27) Barrow, M. J.; Mills, O. S. *J. Chem. Soc. A* **1971**, 864.
(28) Stella, S.; Floriani, C.; Chiesi-Villa, A.; Guastini, C. *J. Chem. Soc., Dalton Trans.* **1988**, 545.
(29) Calligaris, M.; Yoshida, T.; Otsuka, S. *Inorg. Chim. Acta* **1974**, *11*, L15.
(30) Sharp, P. R.; Hoard, W. D.; Barnes, C. L. *J. Am. Chem. Soc.* **1990**, *112*, 2024.
(31) Ang, H. G.; Kwik, W. L.; Ong, K. K. *J. Fluorine Chem.* **1993**, *60*, 43.
(32) Kochi, J. K. *Agnew.Chem., Int. Ed. Engl.* **1988**, *27*, 1227.
(33) Eberson, L. *Adv. Phys. Org. Chem.* **1982**, *18*, 79.
(34) Eberson, L. *Electron Transfer Reactions in Organic Chemistry*; Springer-Verlag: Berlin, 1987.
(35) Burger, B. J.; Bercaw, J. E. In *Experimental Organometallic Chemistry*; Wayda, A. L., Darensbourg, M. Y., Eds.; American Chemical Society: Washington, DC, 1987; Vol. 357, pp 79−98.
(36) Sanchez-Delgado, R. A.; Bradley, J. S.; Wilkinson, G. *J. Chem. Soc., Dalton Trans.* **1976**, 399.
(37) Skoog, S. J.; Jorgenson, A. L.; Campbell, J. P.; Gladfelter, W. L.; Douskey, M.; Munson, E. *J. Organomet. Chem.* **1997**. In press.
(38) Galbraith, H. W.; Degering, F. E.; Hitch, F. E. *J. Am. Chem. Soc.* **1951**, *73*, 1323.
(39) Wheeler, O. H.; Gonzalez, D. *Tetrahedron* **1964**, *20*, 189.
(40) Smith, L. I.; Denyes, R. O. *J. Am. Chem. Soc.* **1936**, *58*, 304.
(41) Newton, A. *J. Am. Chem. Soc.* **1943**, *65*, 2434.

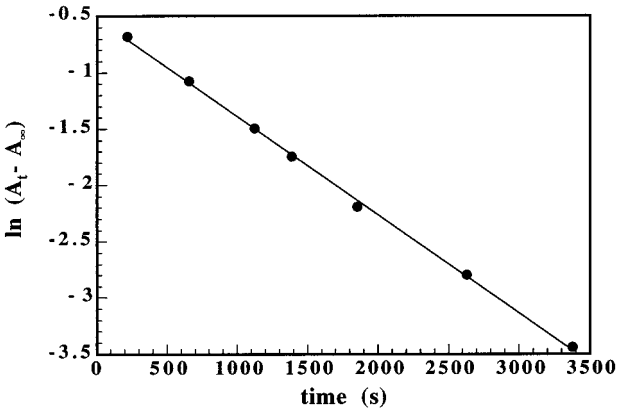

Figure 2. Pseudo-first-order plot for the reaction of $Ru(dppe)(CO)_3$ (**1**) with 4-chloronitrobenzene in THF at 25 °C.

pseudo-first-order rate constants for the deoxygenation were obtained with a precision within ±4%.

Electrochemical Studies. All electrochemical measurements were performed with a Bioanalytical Systems (BAS) Model 100 electrochemical analyzer and were conducted at room temperature. The THF was distilled from lithium aluminum hydride, acetonitrile was distilled from calcium hydride, and both were used immediately. Tetra-*n*-butyl ammonium hexafluorophosphate (TBAH) (Southwestern Analytical Chemicals, Inc.) was dried under vacuum and stored in a desiccator. Electrolyte solutions were deoxygenated with dry, solvent-saturated argon while in the electrochemical cell. No *iR* compensation was used in the electrochemical measurements.

For the experiments using the nitroarenes, a polished Pt working electrode ($A = 0.03$ cm^2), a Pt auxiliary electrode, and a Pt pseudoreference electrode were used. The reversible ferrocenium/ferrocene (Fc^+/Fc) redox couple served as an internal standard[42] for the determination of potentials, which had been observed at 0.56 V vs SCE in THF containing 0.1 M TBAH.[43] The working compartment of the electrochemical cell was separated from the auxiliary compartment by a fritted-glass salt bridge and from the reference compartment by a modified Luggin capillary. Each of the three compartments contained 0.1 M solution of supporting electrolyte, and the working compartment contained ca. 1 mM substrate.

Experiments using metal complexes were carried out in a 0.3 M TBAH THF solution using a normal three-electrode configuration. The experiments employed a polished glassy-carbon-disc working electrode ($A = 0.07$ cm^2), a freshly prepared BAS nonaqueous reference electrode (the Ag wire was immersed in a 0.01 M $AgNO_3$ 0.3 M TBAH acetonitrile solution), and a Pt auxiliary electrode. Under these conditions the potential for the Fc^+/Fc couple was observed at 0.16 V vs $Ag/AgNO_3$ and potentials reported relative to SCE were related to this couple. The uncompensated resistance of the THF/0.3 M TBAH solution was minimized by using a range of slow sweep rates from 0.01 to 0.1 V s^{-1}. The measurements of shifts in peak potentials were also done using a cobaltocene redox couple known to behave reversibly, as an internal standard.[44] The area of the electrode was checked by performing chronocoulometry experiments on a ferrocene standard.[45a] Passivation of the electrode was observed after the initial scan, and this complication was mitigated by polishing the electrode after each experiment.

Synthesis of $Ru(dppe)(CO)_2[ON(4\text{-}Cl\text{-}2\text{-}CF_3C_6H_3)]$ (2a). Compound **1** (0.28 g, 0.48 mmol) was loaded into a 25 mL reaction flask. The 4-chloro-2-(trifluoromethyl)nitrobenzene (0.328 g, 1.45 mmol in 10 mL of THF) solution was prepared separately, degassed by bubbling with dry nitrogen, and added to the reaction flask via cannula. The reaction mixture turned from light yellow to a dark red and was kept at 0 °C until the starting materials were fully reacted as monitored by FTIR. The reaction was complete after about 10−15 min. The THF was then removed under vacuum until ca. 3 mL of reaction mixture remained. The reaction mixture was cooled to −78 °C, and freshly distilled hexane (20 mL) was added via syringe, and the reaction mixture stirred rapidly. A dark orange/red precipitate formed, which was collected on a glass frit at −78 °C, washed several times with hexane, and dried under a flow of dry nitrogen or under vacuum to give **2a** in 68% isolated yield. IR (cm^{-1}, KBr): ν_{CO} 2028 (s), 1960 (s). ^{1}H NMR (ppm, CD_2Cl_2): δ 2.20 (m, CH_2), 2.66 (m, CH_2), 7.25 (m, ArH), 7.32 (m, ArH), 7.40 (m, ArH), 7.58 (m, ArH), 7.63 (m, ArH), 6.96 (m, ArH), 8.06 (m, ArH). $^{31}P\{^1H\}$ NMR (ppm, CD_2Cl_2): δ 69.4 (d, $J_{PP} = 18.2$ Hz), 51.1 (d, $J_{PP} = 18.1$ Hz). $^{13}C\{^1H\}$ NMR (ppm, CD_2Cl_2): δ 24.97 (dd, $J_{CP1} = 16$ Hz, $J_{CP2} = 31.7$ Hz, CH_2), 28.17 (dd, $J_{CP1} = 11.1$ Hz, $J_{CP2} = 28.0$, CH_2), 116.6 (q, $J_{CF} = 30.55$ Hz), 124 (q, $J_{CF} = 273.4$ Hz, CF_3), 165.8 (s, ipso C), 191.6 (dd, $J_{C1P2} = 7.57$ Hz, $J_{C1P1} = 112.3$ Hz, CO), 198.6 (d, $J_{C2P} = 13.42$ Hz, CO). ^{19}F NMR (ppm, CD_2Cl_2) δ −59.89 (s, CF_3). FAB mass spectrum (Ru^{102}) P (*m*/*e*) 765.9. Anal. Calcd for $Ru(dppe)(CO)_2[ON(C_7H_3ClF_3)]\cdot CH_2Cl_2$: C, 50.89; H, 3.44; N, 1.65. Found: C, 50.68; H, 3.56; N, 1.69.

Synthesis of $Ru(dppe)(CO)_2[ON(4\text{-}CF_3C_6H_4)]$ (2b). The same procedure was used to make **2b**, except a precooled THF/nitroarene solution was added at 0 °C. The reaction was complete within 20−30 min. Care was taken to isolate the product as quickly as possible to avoid decomposition. A similar isolation procedure gave **2b** in 65% isolated yield. Subsequent recrystallization from hexane/CH_2Cl_2 (10/1) produced analytically pure material. IR (cm^{-1}, KBr): ν_{CO} 2029 (s), 1950 (s). ^{1}H NMR (ppm, CD_2Cl_2): δ 2.37 (m, CH_2), 2.86 (m, CH_2) 7.43 (m, ArH), 7.66 (m, ArH), 8.08 (m, ArH), 8.28 (m, ArH). $^{31}P\{^1H\}$ NMR (ppm, CD_2Cl_2): δ 62.69 (d, $J_{PP} = 17.12$ Hz), 48.62 (d, $J_{PP} = 17.12$ Hz). $^{13}C\{^1H\}$ NMR (ppm, CD_2Cl_2): δ 27.45 (dd, $J_{CP1} = 24.4$ Hz, $J_{CP2} = 39.07$ Hz, CH_2), 29.1 (dd, $J_{CP1} = 19.46$ Hz, $J_{CP2} = 37.7$, CH_2), 118.6 (q, $J_{CF} = 31.7$ C4), 172.26 (s, ipso C), 192.15 (dd, $J_{C1P2} = 9.73$ Hz, $J_{C1P1} = 112.3$ Hz, CO), 198.3 (d $J_{C2P} = 14.63$ Hz, CO). ^{19}F NMR (ppm, CD_2Cl_2) δ −57.13 (s, CF_3). IS mass spectrum (Ru^{102}) P (*m*/*e*) 732.0 Anal. Calcd for $Ru(dppe)(CO)_2[ON(C_7H_4F_3)]\cdot CH_2Cl_2$: C, 57.37; H, 4.01; N, 1.86. Found: C, 57.31; H, 4.08; N, 1.85.

Synthesis of $Ru(dppe)(CO)_2[ON(2\text{-}CF_3C_6H_4)]$ (2c). The same procedure as used for **2b** was employed, except that the reaction took 3 h to complete at 0 °C. Compound **2c** was isolated in 60% yield. Subsequent recrystallization from hexane/CH_2Cl_2 (10/1) at −78 °C gave the pure material. IR (cm^{-1}, THF): ν_{CO} 1957 (s), 2025 (s). ^{1}H NMR (ppm, CD_2Cl_2): δ 2.32 (m, CH_2), 2.69 (m, CH_2), 6.73 (t, $J_{HH} = 7.2$ Hz, ArH), 7.39 (m, ArH), 7.63 (m, ArH), 8.00 (m, ArH), 8.11 (m, ArH). $^{31}P\{^1H\}$ NMR (ppm, CD_2Cl_2): δ 62.17 (d, $J_{PP} = 17.96$ Hz), 43.21 (d, $J_{PP} = 17.96$ Hz). $^{13}C\{^1H\}$ NMR (ppm, CD_2Cl_2): δ 28.71 (dd, $J_{CP1} = 11.09$ Hz, $J_{CP2} = 29.94$ Hz), 25.42 (dd, $J_{CP1} = 15.23$ Hz, $J_{CP2} = 31.14$ Hz), 116.6 (q, $J_{CF} = 29.93$ Hz, CH), 125.57 (q, $J_{CF} = 273.4$, CF_3) 167.22 (d, 2.79 Hz), 192.18 (dd, $J_{C1P2} = 11.01$ Hz, $J_{C1P1} = 113.56$ Hz, CO), 199.05 (d, $J_{C2P} = 12.82$ Hz, CO). ^{19}F NMR (ppm relative to $CFCl_3$, CD_2Cl_2): δ −61.37. FAB mass spectrum (Ru^{102}) P (*m*/*e*): 732.0. Anal. Calcd for $Ru(dppe)(CO)_2(ON(C_7H_4F_3)\cdot CH_2Cl_2$: C, 57.37; H, 4.01; N, 1.86. Found: C, 56.94; H, 4.40; N, 1.81.

NMR Spectroscopy of $Ru(dppe)(CO)_2[ON(Ar)]$. Transfer and handling of the compounds while in solution and during the NMR spectral experiments were carried out between −35 to −78 °C to minimize decomposition. Samples were loaded into NMR tubes attached to ground glass joints in the glovebox. The tubes were then capped with Teflon valves, removed from the glovebox, and deuterated methylene chloride was vacuum distilled into the NMR tube at −78 °C. The tube was then cooled to −196 °C and sealed. A typical NMR sample would contain 1.0 mmol of $Ru(dppe)(CO)_2[ON(Ar)]$ in 0.4 mL of solvent.

X-ray Crystallography of $Ru(dppe)(CO)_2[ON(4\text{-}Cl\text{-}2\text{-}CF_3C_6H_3)]$ (2a). Dark red prisms of $RuC_{36}P_2NO_3F_3Cl_3H_{27}$ were grown from hexane/dichloromethane. A suitable crystal was removed from a Schlenk flask and quickly covered with oil, transferred to the tip of a glass fiber, mounted on the goniometer of a CAD-4, and cooled to −100 °C with an Enraf-Nonius FR558SH low-temperature device. Table 1 provides the details of the structural analysis. The search routine collected 25 reflections at low angles that provided an initial cell. A search along the axes provided higher angle reflections between

(42) Gagné, R. R.; Koval, C. A.; Lisensky, G. C. *Inorg. Chem.* **1980**, *19*, 2854.
(43) Geiger, W. E. In *Organometallic Radical Processes*; Trogler, W. C., Ed.; Elsevier: Amsterdam, 1990; pp 142−172.
(44) Geiger, W. E. *Prog. Inorg. Chem.* **1985**, *33*, 275.
(45) Adams, R. A. *Electrochemistry at Solid Electrodes*; Marcel Dekker: New York, 1969; (a) p 221, (b) p 126.

Table 1. Summary of Crystallographic Data

Crystal Parameters	
compound	$Ru(dppe)(CO)_2[\eta^2\text{-}ON(C_6H_3ClCF_3)]\cdot CH_2Cl_2$
crystal system	monoclinic
space group	$P2_1/c$ (#14)
formula	$RuC_{36}P_2NO_3F_3Cl_3H_{29}$
formula weight, g mol^{-1}	847.99
a, Å	14.556(8)
b, Å	12.903(6)
c, Å	20.102(1)
α, deg	90
β, deg	105.60(6)
γ, deg	90
V, Å^3	3636(8)
Z	4
ρ(calcd), g cm^{-3}	1.549
temp, °C	−100
abs coeff, cm^{-1}	7.816
cryst dimens, mm	0.700 × 0.570 × 0.260
trans. factors, max to min %	1.00−0.71
abs corr applied	ψ-scan
Measurement of Intensity Data	
diffractometer	Enraf-Nonius CAD-4
radiation	Mo Kα (λ = 0.710 69 Å)
monochromator	graphite crystal
programs used	TEXSAN
method of structure solution	Patterson Method
scan type	ω
scan range, deg	0−52
no. of reflns measd	7879
no. of unique reflns	7420
no. of reflns used	4016
residual peaks, e/Å	1.13 and −1.04
cutoff	3.00σ
p	0.03
R	0.065
R_w	0.068
error in observation of unit weight	1.91

20° and 52° in 2θ that were carefully centered and refined to give the final cell constants and orientation matrix. At this time, a check was performed for a higher symmetry unit cell; none was found. Omega scans were collected in one shell to 18° using a prescan speed of 16.48° min^{-1} and from 18−24° at 4.1° min^{-1}. Three strong reflections were chosen as intensity checks and monitored every hour during data collection. No decay was observed. Six reflections between 19° and 52° in 2θ were chosen as orientation checks and were monitored every 400 reflections during data collection.

The data were processed and the structure solved and refined using the TEXSAN 5.0 series of programs.[46] Systematic absences uniquely defined the space group as $P2_1/c$ (#14). The ruthenium atom was found by the Patterson method, and the other nonhydrogen atoms by Fourier techniques and the direct methods program DIRDIF. After a full isotropic refinement, the hydrogen atoms were placed in idealized positions with d_{CH} = 0.95 Å, and B values 20% greater than the B_{eq} of the carbon to which they were bonded. Their positions were updated every cycle of least squares refinement using a riding model; they were not refined but were included in the structure factor calculation. The asymmetric unit contains a molecule of dichloromethane that appears to be partially disordered. The chlorine and carbon atoms were located in the difference map and refined, but the hydrogen atoms were omitted. After isotropic refinement of this model, redundant data were averaged. Full anisotropic refinement of all nonhydrogen atoms using full-matrix least squares was performed and converged to a final R = 0.065 (2σ). The final difference map was essentially flat, with maximum and minimum peaks of 1.13 and −1.04 e Å^{-3}. An absorption correction was applied before solution and refinement using the ψ-scan technique.

(46) TEXSAN 5.0, Molecular Structure Corporation: The Woodlands, TX.

Table 2. Bond Distances[a] in $Ru(dppe)(CO)_2[\eta^2\text{-}ON(C_6H_3ClCF_3)]$

A. Metal−Ligand Distances			
Ru1−P1	2.401(3)	Ru1−P2	2.333(3)
Ru1−O3	2.054(6)	Ru1−N1	2.115(7)
Ru1−C1	1.918(9)	Ru1−C2	1.88(1)
B. Intraligand Distances			
P1−C21	1.837(9)	P1−C31	1.83(1)
P1−C41	1.82(1)	P2−C22	1.83(1)
P2−C51	1.82(1)	P2−C61	1.82(1)
O1−C1	1.12(1)	O2−C2	1.15(1)
O3−N1	1.412(9)	N1−C11	1.42(1)
F1−C17	1.33(1)	F2−C17	1.37(1)
F3−C17	1.33(1)	C11−C12	1.39(1)
C11−C16	1.42(1)	C12−C13	1.37(1)
C12−C17	1.52(1)	C13−C14	1.39(1)
C14−C15	1.35(1)	C15−C16	1.36(1)
C21−C22	1.53(1)	C31−C32	1.40(1)
C31−C36	1.39(1)	C32−C33	1.35(1)
C33−C34	1.39(2)	C34−C35	1.35(1)
C35−C36	1.40(1)	C41−C42	1.38(1)
C41−C46	1.39(1)	C42−C43	1.37(1)
C43−C44	1.36(2)	C44−C45	1.39(2)
C45−C46	1.35(1)	C51−C52	1.38(1)
C51−C56	1.39(1)	C52−C53	1.37(1)
C53−C54	1.39(1)	C54−C55	1.37(1)
C55−C56	1.38(1)	C61−C62	1.39(1)
C61−C66	1.36(1)	C62−C63	1.36(1)
C63−C64	1.39(2)	C64−C65	1.36(2)
C65−C66	1.41(2)	CL1−C14	1.76(1)

[a] In angstroms.

Scattering factors were taken from the usual sources,[47] and the effects of anomalous dispersion were included for the nonhydrogen atoms.[48] The bond distances and angles are listed in Tables 2 and 3, respectively. Figure 3 shows the molecular structure of $Ru(dppe)(CO)_2[ON(4\text{-}Cl\text{-}2\text{-}CF_3C_6H_3)]$.

Results

The ruthenium complex **1** reacts with nitroarene, to form CO_2 and a side-bound ruthenium nitrosoarene complex **2**.[22] The current study describes the isolation and characterization of **2**, as well as detailed kinetic studies on the deoxygenation reaction shown in eq 4.

Synthesis and Characterization of $Ru(dppe)(CO)_2[\eta^2\text{-}ON(Ar)]$ (where Ar = 4-Chloro-2-(trifluoromethyl)phenyl (2a), 4-(Trifluoromethyl)phenyl (2b), and 2-(Trifluoromethyl)-phenyl (2c)). Due to rapid decomposition on the reaction time scale, the nitrosoarene complex was not usually isolated. The concentration of dark red product was found, however, to build up to a larger degree in the reactions involving highly electron deficient nitroarene compounds. When 2- or 4-(trifluoromethyl)nitrobenzene was used, the rate of product formation was found to be equal to the rate of disappearance of the starting complex **1** at 25 °C. This finding led to the development of a synthetic procedure for isolating products using electron deficient nitroarenes. The nitrosoarene complex **2b** was isolable in ca. 60−70% yield but lacked sufficient stability for convenient manipulation. With 4-chloro-2-(trifluoromethyl)nitrobenzene, the resulting nitrosoarene complex **2a** was isolated and ultimately crystallized from hexane/CH_2Cl_2 at low temperature. The infrared spectrum of **2** in the ν_{CO} region showed two bands at ca. 2028 cm^{-1} and 1960 cm^{-1}, which is typical for neutral *cis*-dicarbonyl Ru^{2+} species.[8] The proton NMR spectrum for **2** exhibited a downfield shift of the aromatic protons compared

(47) Cromer, D. T.; Waber, J. T. In *International Tables for X-Ray Crystallography;* Kynoch Press: Birmingham, England, 1974; Vol. IV, Table 2.2A.

(48) Cromer, D. T. In *International Tables for X-Ray Crystallography*; Kynoch Press: Birmingham, England, 1974; Vol. IV, Table 2.3.1.

Table 3. Bond Angles (deg) for Ru(dppe)$(CO)_2$-[η^2-ON($C_6H_3ClCF_3$)]

A. Ligand−Metal−Ligand			
P1−Ru1−P2	82.5(1)	P1−Ru1−O3	92.3(2)
P1−Ru1−N1	94.2(2)	P1−Ru1−C1	172.3(3)
P1−Ru1−C2	86.4(3)	P2−Ru1−O3	108.6(2)
P2−Ru1−N1	148.0(2)	P2−Ru1−C1	91.1(3)
P2−Ru1−C2	93.7(4)	O3−Ru1−N1	39.5(2)
O3−Ru1−C1	93.8(3)	O3−Ru1−C2	157.3(4)
N1−Ru1−C1	93.5(4)	N1−Ru1−C2	117.9(4)
C1−Ru1−C2	89.7(4)		
B. Metal Carbonyls and Phosphines			
Ru1−P1−C21	104.9(3)	Ru1−P1−C31	116.4(3)
Ru1−P1−C41	120.1(3)	C21−P1−C31	105.9(4)
C21−P1−C41	102.0(4)	C31−P1−C41	105.7(4)
Ru1−P2−C22	109.6(3)	Ru1−P2−C51	117.7(3)
Ru1−P2−C61	116.2(3)	C22−P2−C51	104.6(4)
C22−P2−C61	104.5(5)	C51−P2−C61	102.8(4)
Ru1−C1−O1	173.8(9)	Ru1−C2−O2	175(1)
P1−C21−C22	107.1(6)	P2−C22−C21	111.6(6)
P1−C31−C32	122.7(8)	P1−C31−C36	118.1(7)
C32−C31−C36	119.3(9)	C31−C32−C33	120(1)
C32−C33−C34	120(1)	C33−C34−C35	122(1)
C34−C35−C36	119(1)	C31−C36−C35	120.4(9)
P1−C41−C42	120.4(8)	P1−C41−C46	122.0(7)
C42−C41−C46	117.3(9)	C41−C42−C43	122(1)
C42−C43−C44	120(1)	C43−C44−C45	119(1)
C44−C45−C46	120(1)	C41−C46−C45	121(1)
P2−C51−C52	122.2(7)	P2−C51−C56	119.8(7)
C52−C51−C56	118.0(9)	C51−C52−C53	122.1(9)
C52−C53−C54	119.3(9)	C53−C54−C55	119(1)
C54−C55−C56	121.2(9)	C51−C56−C55	120.0(9)
P2−C61−C62	120.7(7)	P2−C61−C66	120.1(8)
C62−C61−C66	119(1)	C61−C62−C63	121(1)
C62−C63−C64	120(1)	C63−C64−C65	119(1)
C64−C65−C66	121(1)	C61−C66−C65	120(1)
C. [η^2-ON($C_6H_3ClCF_3$)]			
Ru1−O3−N1	72.5(4)	Ru1−N1−O3	67.9(4)
Ru1−N1−C11	119.2(6)	O3−N1−C11	112.2(7)
N1−C11−C12	122.5(8)	N1−C11−C16	120.3(9)
C12−C11−C16	116.9(9)	C11−C12−C13	122.0(9)
C11−C12−C17	120.6(8)	C13−C12−C17	117.3(9)
C12−C13−C14	118.8(9)	CL1−C14−C13	118.1(8)
CL1−C14−C15	121.3(8)	C13−C14−C15	120.6(9)
C14−C15−C16	121.0(9)	C11−C16−C15	120.7(9)
F1−C17−F2	106.8(9)	F1−C17−F3	106.6(9)
F1−C17−C12	113.1(9)	F2−C17−F3	106.2(9)
F2−C17−C12	111.1(9)	F3−C17−C12	112.6(9)

to the starting nitroarene, and characteristic multiplets appeared at 2.66 ppm for the dppe methylene groups. A pair of doublets was observed in the $^{31}P\{^1H\}$ NMR spectrum at 69 ppm (d, J_{PP} = 18.2 Hz) and 51 ppm (d, J_{PP} 18.1 Hz) indicating nonequivalent phosphorus atoms. The $^{13}C\{^1H\}$ NMR spectrum for **2** exhibited resonances at 191 ppm (dd, J_{C1P2} = 7.57 Hz, J_{C1P1} = 112.3 Hz), and 198 ppm (d, J_{C2P} = 13.42 Hz), which was consistent with one carbonyl located cis to one P atom and trans to the other, while the other carbonyl was located cis to both P atoms. The peak at 198.3 ppm appeared as a doublet, apparently because a coupling constant to one of the P ligands was too small to resolve.

Structural Analysis of Ru(dppe)$(CO)_2$[ON(4-Cl-2-$CF_3C_6H_3$)]. Single-crystal X-ray crystallographic analysis demonstrated that in the solid state the complex **2a** contained an η^2-ArNO ligand. The complex exhibited a slightly distorted octahedral structure of Ru^{2+}. The Ru−C bond trans to the phosphine ligand, Ru−C1 = 1.918(9) Å, was slightly longer than the Ru−C bond trans to the oxygen of the nitroso ligand Ru−C2 = 1.88(1) Å; the observed trans effect as well as similar dppe bite angles (82.5(1)°) have been observed in other complexes with the same Ru(dppe)$(CO)_2$ fragment.[8,9]

The nitrogen in the ruthenaoxaziridine ring was pyramidal, and the N−O bond length (1.412(9) Å) was slightly shorter than the single bond in hydroxylamine (1.46 Å).[49] The N−O length was similar to that of other monometallic complexes containing side-bound nitroso ligands: oxo(phenylnitroso)-(pyridine-2,6-dicarboxylato) (hexamethylphosphoramide)molybdenum(VI) (1.416(7) Å),[23] bis(triphenylphosphine)(phenylnitroso)platinum(II) (1.410(7) Å),[24] (pentamethylcyclopentadienyl)(phenylimido)(phenylnitroso)phenyltungsten(VI) (1.432(6) Å),[25] and tetraphenylphosphonium tetracyanooxo[*N*-*o*-tolylhydroxylaminato(2−)-*O*,*N*]molybdate(VI) (1.393(10) Å).[26] The phenyl ring of the nitroso ligand was directed away from the dppe ligand to minimize steric interactions between the aromatic rings. The ortho trifluoromethyl group was also directed away from the oxygen of the nitroso ligand. Given the similarity between the N−O bond lengths of the nitroso ligand and that of hydroxylamine, we suggest that the nitroso ligand should be considered dianionic and the metal center considered a d^6 Ru^{2+}.

Electrochemical Studies. Reversible one-electron reduction was observed for nitroarenes in THF using a scan rate of 50 mV/s (i_{pc}/i_{pa} = 1.01 ± 0.02), where $\Delta E_p = E_{pc} - E_{pa}$ and peak currents were comparable to that observed for the Fc^+/Fc couple under identical conditions. The trend in the standard reduction potentials for different nitroarenes ($E°_{ArNO2} = (E_{pc} + E_{pa})/2$) paralleled values obtained by previous workers where reversible one electron reduction (eq 5) was reported in acetonitrile,[50]

$$ArNO_2 \underset{-e^-}{\overset{+e^-}{\rightleftharpoons}} ArNO2^{\bullet -} \qquad (5)$$

DMF,[51] and DMSO.[52]

Correlation between reduction potentials and σ values was observed for meta (CH_3, Cl) and para (Me_2N, OCH_3, CH_3, H, Cl, CF_3) substituted nitroarenes (ρ = +0.34). The reduction potentials became more negative for nitroarenes containing electron donating substituents and for ortho substituted nitroarenes. The changes in the reduction potentials measured in THF between 4-CH_3 and 2-CH_3, or 2,6-$(CH_3)_2$ substituted nitroarenes were typical of the changes caused by a steric barrier preventing the nitro group from becoming coplanar to the aryl ring.[53] The reduction of dinitrodurene was chemically irreversible at a scan rate of 50 mV s^{-1}, and no return anodic wave was observed. The potential was estimated from the data of Maki and Geske[54] who reported a reversible potential for dinitrodurene at a mercury electrode that was close to dinitromesitylene.

Oxidation of **1** was chemically irreversible up to scan rates (υ) of 1.0 V s^{-1}. After initial oxidation (E_{pa} = −0.07 V vs $Ag/AgNO_3$, υ = 0.1 V s^{-1}) a return cathodic wave was observed at −1.0 V vs $Ag/AgNO_3$ (Figure 4a) which corresponded to the reduction of the dimer $[Ru_2(dppe)_2(CO)_6]^{2+}$. The wave at −1.0 V was absent if potential was swept from −0.5 to −1 V indicating that the dimer was generated from the oxidation of **1**. The assignment of the reduction wave as that of the dimer was confirmed by placing an isolated sample of the dimer under identical conditions and reducing it (E_{pc} = −1.0 V) to form **1** (E_{pa} = −0.09 V) (Figure 4b).

Complex **1** exhibited a peak width ($E_p - E_{p/2}$) of 58 ± 4 mV, which agrees reasonably well with the value (57 mV)

(49) Giguère, P. A.; Liu, I. D. *Can. J. Chem.* **1952**, *30*, 948.
(50) Maki, A. H.; Geske, D. H. *J. Am. Chem. Soc.* **1961**, *83*, 1852.
(51) Holleck, L.; Becher, D. *J. Electroanal. Chem.* **1962**, *4*, 321.
(52) Geer, R. D.; Byker, H. J. *J. Org. Chem.* **1982**, *47*, 1662.
(53) Zuman, P. *Substituent Effects in Organic Polarography*; Plenum Press: New York, 1967.
(54) Geske, D. H.; Ragle, J. L.; Bambenek, M. A.; Balch, A. L. *J. Am. Chem. Soc.* **1964**, *86*, 987.

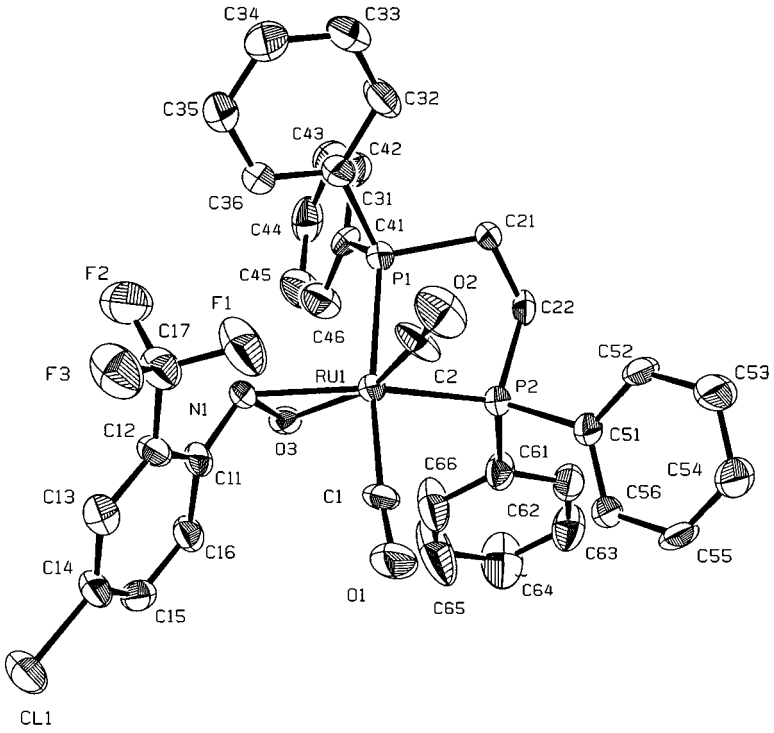

Figure 3. ORTEP of Ru(dppe)$(CO)_2$[ON(2-CF_3,4-Cl,C_6H_3)] (**2a**). Thermal ellipsoids are drawn at the 40% level, and hydrogen atoms are omitted for clarity.

expected for an electrochemically reversible one-electron charge transfer.[45b] A scan rate study on a 0.51 mM solution found the peak current i_{pa} to vary linearly with $v^{1/2}$ within the range 0.01 V $s^{-1} \leq v \leq 0.1$ V s^{-1} yielding a slope of 3.1×10^{-5} A $V^{-1/2}$ $s^{-1/2}$ ($r = 0.998$) and a zero intercept, thus $n^{3/2}D^{1/2} = 3.2 \times 10^{-3}$ cm $s^{-1/2}$.[55a] A potential step experiment from -0.20 V to 0.0 V vs $Ag/AgNO_3$ using a pulse width of 250 ms yielded a linear Anson plot[55b] ($r = 0.999$) with a slope of 1.18×10^{-5} C $s^{-1/2}$ for a 0.582 mM solution. From the slope, a value of $nD^{1/2}$ of 2.66×10^{-3} cm $s^{-1/2}$ was obtained. A calculation of the diffusion coefficient from the molecular volume using the Stokes−Einstein equation[56] gave $D = 8.7 \times 10^{-6}$ cm^2 s^{-1}, which was in agreement with the experimentally determined value from both the scan rate study and the chronocoulometry experiments (1.0×10^{-5} and 7.1×10^{-6} cm^2 s^{-1}, respectively) if n was assumed to be one.

A systematic positive shift in the anodic peak potential (E_{pa}) with scan rate was observed relative to E_{pa} of cobaltocene, and the plot of ΔE_{pa} vs log v was linear for v from 0.01 to 1.0 V s^{-1} with a slope of 19.6 ± 2 mV, which is close to the theoretical value of 19.7 predicted for a one-electron oxidation followed by a rapid dimerization reaction.[57] The difference in the peak potentials of Ru(dppe)$(CO)_3$ in Figures 4a,b was consistent with a concentration dependence on the peak potential expected for a follow-up dimerization reaction. On the basis of these studies we conclude that the oxidation of **1** occurs with a diffusion-controlled, reversible charge transfer (eq 6)[58−60] accompanied

$$\text{Ru(dppe)(CO)}_3 \underset{+e^-}{\overset{-e^-}{\rightleftharpoons}} \text{Ru(dppe)(CO)}_3^{\bullet+} \qquad (6)$$

by a fast follow-up dimerization (eq 7).

$$[\text{Ru(dppe)(CO)}_3]^{\bullet+} \xrightarrow{\text{fast}} {}^1/_2[\text{Ru}_2\text{(dppe)}_2\text{(CO)}_6]^{2+} \qquad (7)$$

Under the same conditions a linear correlation between $E°$ of variously substituted bis(phosphine) tricarbonyl ruthenium complexes ($RuL_2(CO)_3$) and pKa was observed over a range of 7 pKa units.[61] An estimate for $E°_1$ (-0.027 V vs $Ag/AgNO_3$ or 0.37 vs SCE) was obtained from interpolation using the pKa of dppe (4.9). Similar trends were observed for the oxidation of isoelectronic $[MnL_2(CO)_3]^-$ complexes.[62]

Kinetic Results. The kinetic runs were carried out in the absence of CO to simplify the IR spectrum during the progress of the reaction. The rates of reaction were obtained by monitoring the disappearance of **1** by FTIR spectroscopy, in the presence of at least a ten fold excess of nitroarene. In the presence of CO, the four-membered metallacycle (eq 2) would form as the insertion product from **2**; however, the rate of disappearance of **1** was not affected by the presence of CO. A kinetic run carried out in a CO-saturated THF solution of 4-chloronitrobenzene (0.0552 M), and **1** (5.31 mM) gave the second-order rate constant $k_2 = 2.08 \pm 0.04 \times 10^{-2}$ M^{-1} s^{-1}, which was comparable to reaction rates measured without CO. The kinetic runs carried out in a saturated CO solution were further complicated by the presence of trace amounts of water from the gaseous CO. The presence of water regenerated **1** and produced 4-chloroaniline (detected by GPC) as an organic

(55) Bard, A. J.; Faulkner, L. R. *Electrochemical Methods*; John Wiley & Sons: New York, 1980; (a) p 218, (b) p 200.

(56) The diffusion coefficients can be calculated from the Stokes−Einstein equation $D = kT/6\pi\eta r$ where η is the viscosity of THF at 25 °C (0.466 cP from Daubert, T. E.; Danner, R. P. *Physical and Thermodynamic Properties of Pure Chemicals: Data Compilation*; Taylor & Francis: Washington, DC, 1989), k is the Boltzman constant, T is the absolute temperature (298.15 K) and r is the radius of **1**. The average radius of **1** was calculated from the density (ρ) measured from X-ray crystallographic analysis using $r = (3MW/N_o\pi\rho 4)^{1/3}$ where MW is the molecular weight of **1**, N_o is Avogadro's number, and ρ is the density of **1** (1.482 g cm^{-3} from ref 37) ($r_1 = 5.4$ Å).

(57) Nadjo, L.; Savéant, J. M. *J. Electroanal. Chem.* **1973**, *48*, 113.

(58) Nicholson, R. S.; Shain, I. *Anal. Chem.* **1964**, *36*, 706.

(59) Klingler, R. J.; Kochi, J. K. *J. Phys. Chem.* **1981**, *85*, 1731.

(60) Klingler, R. J.; Kochi, J. K. *J. Am. Chem. Soc.* **1980**, *102*, 4790.

(61) Skoog, S. J.; Tabakovic, I.; Gladfelter, W. L. *Inorg. Chem.* **1997**. Submitted for publication.

(62) Kochi, J. K. In *Organometallic Radical Processes*; Trogler, W. C., Ed.; Elsevier: Amsterdam, 1990; pp 201−269.

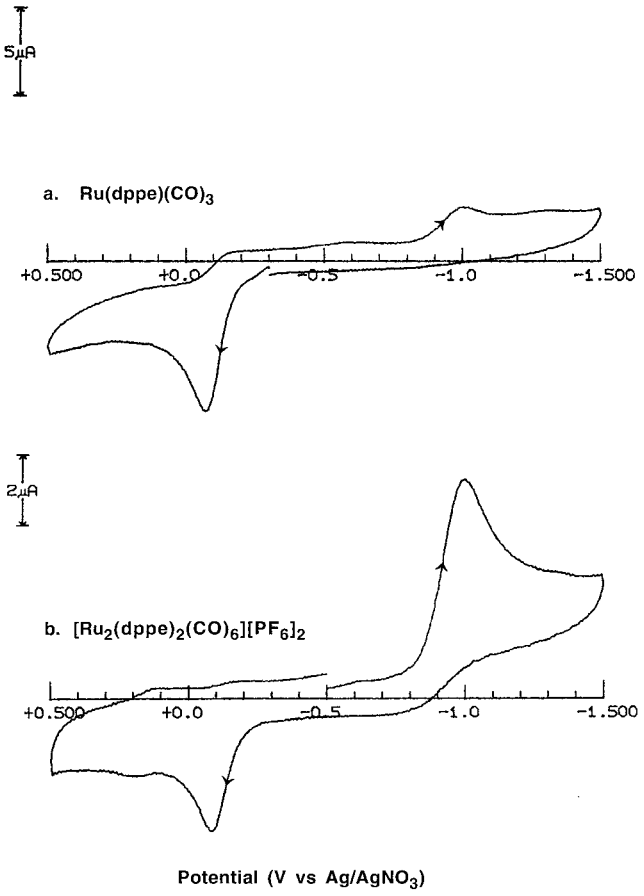

Figure 4. (a) Cyclic voltammogram of 0.58 mM sample of Ru(dppe)-$(CO)_3$ (**1**) in a 0.3 M TBAH THF solution at a scan rate of 0.1 V s^{-1}. The positive scan was initiated at −0.3 V vs $Ag/AgNO_3$. (b) Cyclic voltammogram of a 0.38 mM sample of $Ru_2(dppe)_2(CO)_3(PF_6)_2$ in a 0.3 M TBAH THF solution at a scan rate of 0.1 V s^{-1}. The negative scan was initiated at −0.5 V vs $Ag/AgNO_3$. The feature at 0.16 V is a small amount of ferrocene impurity.

product. These complications were minimized by rigorous drying of the solution over 4 Å molecular sieves; this effect on the rate was smallest at the beginning of the reaction, and rate constants were calculated from data collected within the first two half-lives. Preliminary kinetic runs were carried out using $^{31}P\{^1H\}$ NMR spectroscopy, and comparable rates were observed. Trace amounts of arylazo and arylazoxy compounds were detected in some of the kinetic runs by GPC; similar findings were observed in other work.[14,63]

First-order plots for 1,3,5-triisopropyltrinitrobenzene and dinitrodurene were not linear over the entire course of the reaction. The reaction proceeded faster at the beginning of the run than at the end of the run. About 20% of the starting material reacted within the first 10 h, after this initial period, the reaction would follow pseudo-first-order kinetic behavior. It was suspected that trace amounts of faster-reacting nitroarene impurities were present. No studies were carried out to confirm this hypothesis. The rates for these two nitroarenes were calculated from the later portion of the pseudo-first-order plot, which was linear.

A. Determination of Reaction Order. The reaction was found to be first-order with respect to **1** as seen in Figure 2. The order with respect to nitroarene was determined by varying the concentration of nitroarene over a range of 0.05 M to 4.0 M for nitrobenzene and 0.05 M to 0.5 M for 4-chloronitrobenzene (Table 4). Slopes of 1.07 and 1.21 were observed for 4-chloronitrobenzene and nitrobenzene, respectively, in plots of log k_{obs} vs log [$ArNO_2$] as shown in Figure 5. The deviation from unity in the case of nitrobenzene (dashed line) was attributed to an increase in solvent polarity at high concentrations of nitrobenzene. In the case of the run carried out at 4.0 M nitrobenzene, the solution contained 40% nitrobenzene. The rate increase due to high solvent polarity was corrected using the data obtained in the solvent study (vide infra). The polarity of the reaction medium was calculated by multiplying the percentage of each solvent component by the appropriate polarity factor E_T* [64] to give an effective polarity. This value was used for subtracting the rate increase due to the change in solvent polarity from the experimentally observed rate constant using the empirical relationship derived in the solvent study. When this correction was applied to each rate constant, the slope in the plot of log k_{obs} vs log [nitrobenzene] was reduced to 1.08 and a better linear fit was observed (Figure 5). This effect was absent when using high concentrations of 4-chloronitrobenzene because this nitroarene is less polar than nitrobenzene. The experimentally derived rate expression is shown in eq 8.

$$\text{rate} = \frac{-\mathrm{d}[\mathbf{1}]}{\mathrm{d}t} = k_2[\mathbf{1}][\mathrm{ArNO_2}] \qquad (8)$$

B. Substituent Dependence. The aryl substituents were varied in order to observe rate changes due to structural modification of the nitroarene. A wide range of meta and para

Table 4. Values of k_{obs} and for the Reaction between $Ru(dppe)(CO)_3$ (**1**) and Nitroarene at 25 °C in THF[a]

nitroaromatic	[$ArNO_2$], M	$10^4 k_{obs}$, s^{-1}	$10^4 k_{corr}$,[b] s^{-1}
nitrobenzene	0.0533	0.90 ± 0.01	0.90 ± 0.01
nitrobenzene	0.114	2.04 ± 0.02	1.88 ± 0.02
nitrobenzene	0.174	3.32 ± 0.12	3.06 ± 0.11
nitrobenzene	0.347	7.92 ± 0.12	7.18 ± 0.11
nitrobenzene	0.803	18.8 ± 0.40	16.3 ± 0.34
nitrobenzene	4.07	166 ± 5.7	94.4 ± 3.2
4-chloronitrobenzene	0.0526	8.45 ± 0.2	
4-chloronitrobenzene	0.130	24.9 ± 1.5	
4-chloronitrobenzene	0.205	37.8 ± 2.2	
4-chloronitrobenzene	0.495	95.32 ± 2.6	

[a] $[Ru(dppe)(CO)_3] = 5.31 \times 10^{-3}$ M. [b] Observed rate constant corrected (see results) for solvent polarity changes at high nitrobenzene concentration where E_T* measured for nitrobenzene was 42.0 kcal mol^{-1} (see ref 64).

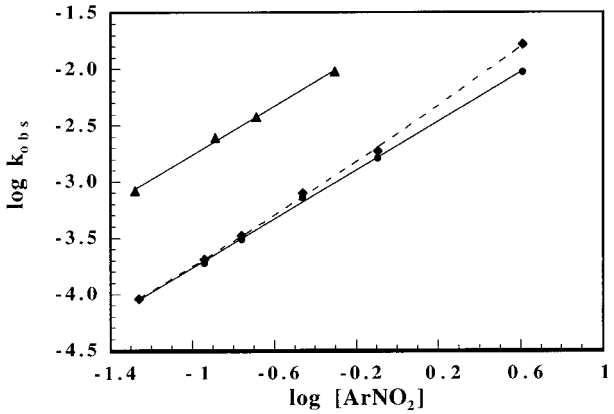

Figure 5. Determination of the order of reaction with respect to 4-chloronitrobenzene (▲), and nitrobenzene (●, ◆) in the reaction with $Ru(dppe)(CO)_3$ (**1**) in THF at 25°C. The dashed line represents data before correcting for the change in solvent polarity.

(63) Vasapollo, G.; Nobile, C. F.; Giannoccaro, P.; Allegretta, F. *J. Organomet. Chem.* **1984**, *277*, 417.

(64) Reichardt, C. *Angew. Chem., Int. Ed. Engl.* **1965**, *4*, 29.

Table 5. Substituent Effects on the Rate of the Initial Deoxygenation of Nitroarene by Ru(dppe)$(CO)_3$ in THF at 25 °C[a]

	nitroarene	[$ArNO_2$], M	10^3k_2, M^{-1} s^{-1}	σ[b]	$E°_{ArNO2}$,[c] V vs SCE	ν_{CO}, cm^{-1}
1	4-$CF_3C_6H_4NO_2$	0.0539	212.0 ± 70.54	0.54	−0.94	2027, 1954
2	3-$ClC_6H_4NO_2$	0.0532	48.1 ± 1	0.37	−1.03	2025, 1951
3	2,3-$Cl_2C_6H_3NO_2$	0.0549	41.7 ± 0.5		−1.04	2025, 1957
4	2-$CF_3C_6H_4NO_2$	0.0539	15.5 ± 0.3		−1.04	2025, 1957
5	4-$ClC_6H_4NO_2$	0.0527	16.3 ± 0.3	0.23	−1.08	2023, 1950
6	2,4,6-(i-Pr)$_3$-$(NO_2)_3C_6$	0.896	0.00426 ± 0.062		−1.10	
7	2-$ClC_6H_4NO_2$	0.0536	3.99 ± 0.062		−1.13	2025, 1955
8	$C_6H_5NO_2$	0.0533	1.68 ± 0.045	0.00	−1.16	2022, 1949
9	3-$CH_3OC_6H_4NO_2$	0.0536	2.20 ± 0.041	0.12	−1.17	2023, 1948
10	3-$CH_3C_6H_4NO_2$	0.0530	0.853 ± 0.013	−0.07	−1.20	
11	4-$CH_3C_6H_4NO_2$	0.0547	0.494 ± 0.015	−0.17	−1.22	
12	2-$C_6H_5C_6H_4NO_2$	0.0697	0.374 ± 0.016		−1.24	2020, 1949
13	dinitromesitylene	0.1402	0.0121 ± 0.00013		−1.27	
14	dinitrodurene	0.294	0.00101 ± 0.00019		−1.27	
15	2-$CH_3C_6H_4NO_2$	0.0540	0.236 ± 0.013		−1.28	
16	4-$CH_3OC_6H_4NO_2$	0.0534	0.143 ± 0.006	−0.27	−1.29	
17	4-$(N(CH_3)_2)C_6H_4NO_2$	0.1459	0.00508 ± 0.0002	−0.83	−1.41	
18	2,6-$(CH_3)_2C_6H_4NO_2$	3.276	0.00113 ± 0.00002		−1.47	

[a] [Ru(dppe)$(CO)_3$] = 5.31×10^{-3} M. [b] Values from ref 65. [c] Cyclic voltammetry carried out in THF with 0.1 M TBAH electrolyte referenced to Fc^+/Fc couple where $E°_{ArNO2} = (E_{pc} + E_{pa})/2$. $E°_1$ (oxidation) for Ru(dppe)$(CO)_3$ was 0.37 V vs SCE.

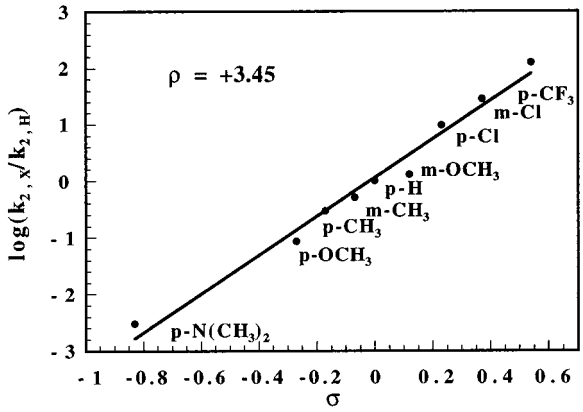

Figure 6. Hammett plot for the reaction between Ru(dppe)$(CO)_3$ (**1**) and meta or para-substituted nitroarenes.

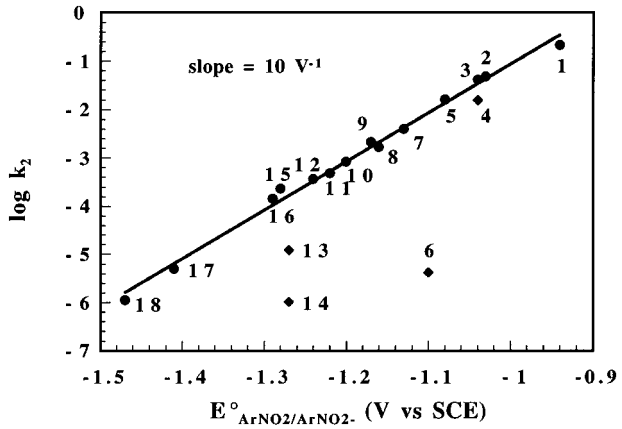

Figure 7. Plot of the second-order rate constants of the deoxygenation reaction of nitroarenes by Ru(dppe)$(CO)_3$ (**1**) in THF at 25°C and $E°_{ArNO_2/ArNO_2^-}$.

substituents were used, from electron-donating *N*,*N*-dimethyl-4-nitroaniline to electron-withdrawing 4-trifluoromethylnitrobenzene. The rate was observed to increase by 1000-fold over this range as seen from Table 5. A ρ value of +3.45 was determined by plotting log ($k_{2,x}/k_{2,H}$) vs σ parameter[65] as shown in Figure 6 where $k_{2,H}$ represents the second-order rate constant for the reaction of **1** with nitrobenzene. The linear fit of the points is remarkably good. The rather large value of ρ indicates buildup of negative charge in the transition state of the rate-determining step of the reaction.

In addition to using para- and meta-substituted nitroarenes, *o*-monosubstituted nitroarenes were studied and exhibited slower rates (Table 5) than the corresponding para-substituted nitroarenes. This behavior paralleled the reduction potential measurements and was caused by the forced rotation of the nitro group out of the plane of the aryl ring. Values of log k_2 for nitroarene substrates correlated to the reduction potentials yielding a slope of 10 V^{-1} as seen in Figure 7.

The rates measured using more highly encumbered nitroarenes (viz., 1,3,5-triisopropyltrinitrobenzene, dinitrodurene, and dinitromesitylene), gave substantially slower rates than predicted on the basis of their reduction potentials. The one structural aspect that all of the highly alkylated nitroarenes had in common was substituents in the ortho and meta positions. This has been referred to as a buttressing effect.[52] Nitroarenes with an ortho methyl substituent lacking a buttressing meta substituent failed to show any rate attenuation. This effect was absent for buttressed chloro substituents; no rate attenuation was observed for 2,3-dichloronitrobenzene. Moderate rate attenuation was observed for 2-trifluoromethylnitrobenzene.

(65) Lowry, T. H.; Richardson, K. S. *Mechanism and Theory in Organic Chemistry*, 3rd ed.; Harper and Row: New York, 1987.

Table 6. Solvent Effects on the Rate of the Deoxygenation of Nitrobenzene by Ru(dppe)$(CO)_3$ at 25 °C[a]

solvent	[$C_6H_5NO_2$], M	10^3k_2, M^{-1} s^{-1}	E_T*,[b] kcal mol^{-1}
tetrahydrofuran	0.0533	1.68 ± 0.045	37.4
dichloromethane	0.0613	6.61 ± 0.088	41.1
dimethylsulfoxide	0.0551	23.1 ± 0.051	45.0

[a] [Ru(dppe)$(CO)_3$] = 5.31×10^{-3} M. [b] Data taken from ref 64.

The product **2** was observed during some of the kinetic runs. The carbonyl stretching frequencies (ν_{CO}) of **2** are given in Table 5. Correlation was observed between σ and ν_{CO} due to varying degrees of carbonyl π back-bonding for compounds containing different aryl groups.

C. Solvent Dependence. The rate of deoxygenation of nitrobenzene was investigated using solvents with varying degrees of polarity to lend further support for charge separation in the transition state of the rate-determining step of the reaction. The rates were measured in tetrahydrofuran, dichloromethane, and dimethyl sulfoxide and are shown in Table 6. The trend in the second-order rate constants followed the solvent polarity as given by the empirical solvent polarity parameter E_T*, which increases in the order: tetrahydrofuran < dichloromethane <

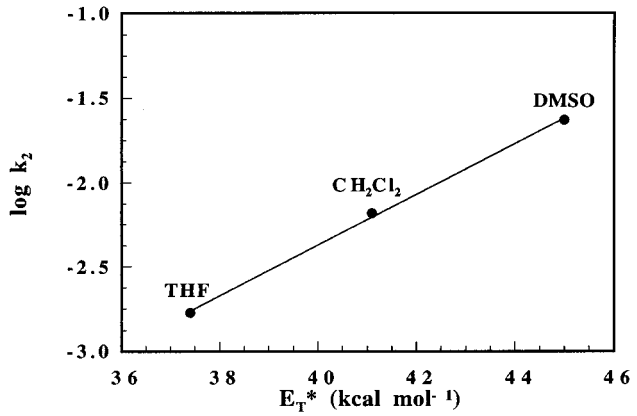

Figure 8. Correlation between the second-order rate constants of the deoxygenation reaction of nitrobenzene by Ru(dppe)$(CO)_3$ (**1**) at 25°C and the Reichardt solvent polarity parameter E_T*.

dimethyl sulfoxide.[64] This trend has been observed for other electron-transfer reactions.[21,66] Excellent correlation was observed by plotting log k_2 vs E_T* (Figure 8), yielding the relationship $\log k_2 = 0.34E_T^* - 19.2$. This empirical relationship was used in correcting for polarity changes in highly concentrated nitrobenzene solutions used in the order determination studies (vide supra).

D. Activation Parameters. The temperature dependence of k_2 for the reaction between **1** and nitroarenes was determined for nitrobenzene, 4-nitrotoluene, 4-chloronitrobenzene, and 2-trifluoromethylnitrobenzene (Table 7). The activation parameters were determined by plotting $\ln(k_2N_oh/RT)$ vs $1/T$ as shown in Figure 9. The negative values of $\Delta S^{\ddagger}$ support a highly ordered transition state and were consistent with a bimolecular mechanism.

E. Attempted Observation of Charge Transfer Complexes. A THF solution containing 3.67 mM of **1** and 0.085 mM of 4-nitrotoluene was prepared in a quartz cuvette and rapidly analyzed by electronic absorption spectroscopy. No new bands were observed, and no change was observed for λ_{max} of the nitroarene. Similar results were obtained with 4-chloronitrobenzene.

Discussion

The initial deoxygenation reaction (eq 4) was shown to be first-order with respect to each reactant, and the product of the reaction was isolated and identified. The ultimate organometallic product of the reaction for the 2-trifluoromethyl-4-chlorophenyl substituent was found to be **2a** using single crystal X-ray diffraction. The other product of the deoxygenation reaction was carbon dioxide, which was observed by IR spectroscopy.

Kinetic experiments carried out in the presence of CO indicate that there was no inhibition of the rate. This evidence, coupled with the previous result that **1** was inert toward ^{13}CO substitution at room temperature,[8] suggests that **1** is the actual reductant in the reaction. There were no intermediates measurable by IR or electronic absorption spectroscopy, and various attempts to trap charged or radical intermediates through hydride- or halogen-atom-transfer reactions were unsuccessful. Previous EPR studies on this system[67] failed to detect any clearly defined radical intermediates suggesting that long-lived, solvent-separated radical-ion pairs were not formed.

Overall the reaction involves ligand substitution, oxygen-atom-transfer from the nitro group to a carbonyl ligand and redox events; any one of which could be rate determining. We can eliminate ligand substitution as a possibility because the rate of exchange with free ^{13}CO at 25 °C was far slower than the observed rate of reaction. Scheme 1 outlines three other reasonable mechanisms for the deoxygenation reaction. Mechanism A depicts oxygen atom transfer via nucleophilic attack on a metal carbonyl and finds precedent in the mechanisms of reaction of Me_3NO with $M(CO)_5$ (where M is a metal in the iron triad) or $M(CO)_6$ (where M is a metal in the chromium triad).[68−70] Mechanism B suggests a rate determining outer-sphere electron transfer to produce the radical cation and anion of Ru(dppe)$(CO)_3$ and $ArNO_2$, respectively. Finally, electron transfer could proceed by an inner-sphere process that could occur concomitantly or follow atom transfer depicted as $\{Ru(dppe)(CO)_3^{+}\cdots ArNO_2^{-}\}$. In the following paragraphs, we will outline the experimental and theoretical considerations that allow us to rule out the first two possibilities and to develop a quantitative correlation of the inner-sphere electron-transfer kinetics to theory.

The rate enhancement induced by electron-withdrawing substituents on the nitroaromatic produces a large positive ρ value that is contrary to what would be expected if the nitroaromatic were acting as a nucleophile in the rate determining step. This is, however, consistent with an electron-transfer mechanism in which the nitroaromatic is the oxidant. Thus, mechanism A was eliminated as a possibility. Differentiation between an outer- or inner-sphere electron transfer relies on a comparison with theory. If outer-sphere electron-transfer theory correctly predicts the observed rate of reaction, we would have no reason to invoke bonding interactions between the oxidant and reductant; however, should the experimental results establish that the rate is faster than predicted for outer-sphere electron transfer, an inner-sphere process would be invoked.

Free Energy Relationship of Kinetic and Thermodynamic Data for Electron Transfer. Marcus theory provides a quantitative method to assess outer-sphere electron-transfer reactions and to evaluate the critical energetic factors contributing to the activation energy. The kinetic scheme used for the analysis of the electron transfer is shown in eqs 9−11.[71] The

$$Ru(dppe)(CO)_3 + ArNO_2 \underset{k_{-diff}}{\overset{k_{diff}}{\rightleftharpoons}} \{Ru(dppe)(CO)_3, ArNO_2\} \quad (9)$$

$$\{Ru(dppe)(CO)_3, ArNO_2\} \underset{k_{-et}}{\overset{k_{et}}{\rightleftharpoons}} \{Ru(dppe)(CO)_3^{\bullet+}, ArNO_2^{\bullet-}\} \quad (10)$$

$$\{Ru(dppe)(CO)_3^{\bullet+}, ArNO2^{\bullet-}\} \xrightarrow{k_p} \text{Products} \quad (11)$$

diffusion rate constant (k_{diff}) represents formation of the precursor complex,[72] k_{-diff} represents the back diffusion rate constant,[73] k_{et} represents the rate constant for electron transfer, k_{-et} represents the back electron-transfer rate constant, and k_p represents the irreversible product-forming rate constant. The assumption that k_p is irreversible is consistent with the data. No EPR active species were observed,[67] and there were no species intercepted by radical ion trapping agents. These

(66) Kosower, E. M.; Mohammad, M. *J. Am. Chem. Soc.* **1968**, *90*, 3271.
(67) Sherlock, S. J.; Boyd, D. C.; Moasser, B.; Gladfelter, W. L. *Inorg. Chem.* **1991**, *30*, 3626.
(68) Alper, H.; Edward, J. T. *Can. J. Chem.* **1970**, *48*, 1543.
(69) Shen, J. K.; Shi, Y. L.; Gao, Y. C.; Shi, Q. Z.; Basolo, F. *J. Am. Chem. Soc.* **1988**, *110*, 2414.
(70) Shen, J. K.; Gao, Y. C.; Basolo, F. *Organometallics* **1989**, *8*, 2144.
(71) Scandola, F.; Balzani, V.; Schuster, G. B. *J. Am. Chem. Soc.* **1981**, *103*, 2519.

Table 7. Activation Parameters for the Deoxygenation of Nitroarene by Ru(dppe)$(CO)_3$ in THF[a]

nitroarene	[$ArNO_2$], M	temperature, °C	10^3k_2, M^{-1} s^{-1}	$\Delta H^{\ddagger}$, kcal mol^{-1}	$\Delta S^{\ddagger}$, eu	$\Delta G^{\ddagger}$,[b] kcal mol^{-1}
2-$CF_3C_6H_4NO_2$	0.0539	25.0	15.5 ± 0.3			
	0.0535	35.0	28.7 ± 0.4			
	0.0539	45.0	46.5 ± 0.8			
	0.0535	55.0	74.4 ± 1.9			
				9.3 ± 0.2	−35.4 ± 0.6	19.8 ± 0.34
4-$ClC_6H_4NO_2$	0.0527	25.0	16.3 ± 0.3			
	0.0549	35.0	30.6 ± 0.6			
	0.0547	45.0	51.0 ± 1.0			
	0.0553	55.0	85.8 ± 2.0			
				9.9 ± 0.1	−33.5 ± 0.4	19.9 ± 0.2
$C_6H_5NO_2$	0.0558	25.0	1.73 ± 0.045			
	0.0543	35.0	3.11 ± 0.03			
	0.0524	45.0	5.92 ± 0.1			
	0.0522	55.0	9.77 ± 0.2			
				10.5 ± 0.3	−36 ± 1	21.3 ± 0.4
4-$CH_3C_6H_4NO_2$	0.0547	25.0	0.494 ± 0.015			
	0.0548	35.0	1.08 ± 0.01			
	0.0544	45.0	1.92 ± 0.01			
	0.0542	55.0	2.99 ± 0.07			
				10.7 ± 0.6	−37 ± 2	21.8 ± 0.8

[a] [Ru(dppe)$(CO)_3$] = 5.31×10^{-3} M. [b] Temperature at 25 °C.

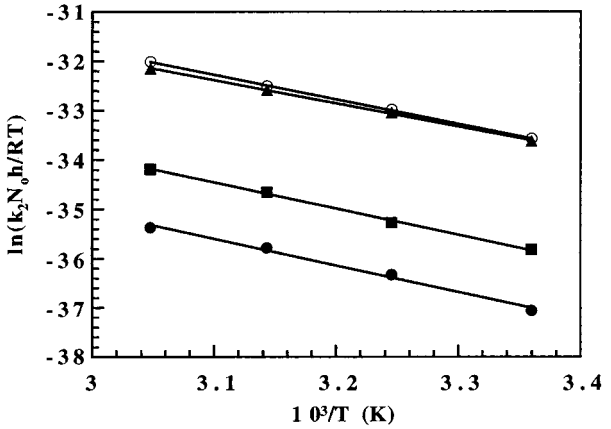

Figure 9. Eyring plot of the second-order rate constant of the deoxygenation reaction of 2-trifluoromethylnitrobenzene (▲), 4-chloronitrobenzene (○), nitrobenzene (■), and 4-nitrotoluene (●), by Ru(dppe)$(CO)_3$ (**1**) in THF from 25 to 55 °C.

Scheme 1

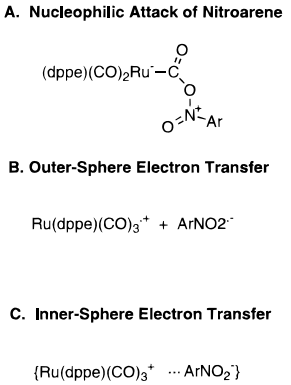

experiments indicated that the radical-ion pair is neither solvent separated nor persistent. Our particular treatment will assume that the electron transfer is irreversible, or more specifically $k_p \gg k_{-et}$. As the diffusion limited rate is so much faster than k_{et} and assuming the steady-state approximation for the precursor complex {Ru(dppe)$(CO)_3$,$ArNO_2$} and the successor complex {Ru(dppe)$(CO)_3^{+\bullet}$,$ArNO_2^{\bullet -}$},[34,71] we set the observed rate constant k_2 equal to k_{et}.

The rate constant for electron transfer (k_{et} in eq 10) can be calculated from theory using equation 12, where the transition probability (κ) is taken as unity, and the collision

$$k_{et} = \kappa Z e^{-\Delta G_{et}^{\ddagger}/RT} \tag{12}$$

frequency Z for a bimolecular reaction is taken as (10^{11} M^{-1} s^{-1}). The activation free energy $\Delta G_{et}^{\ddagger}$ for electron transfer for a neutral donor and acceptor pair can be calculated from Marcus theory[74−76] using the expression shown in eq 13, where $\Delta G^{o\prime}$ is the free energy change associated with eq 10, and the intrinsic barrier ($\Delta G^{\ddagger}(0)$) represents the activation free energy for electron transfer when $\Delta G^{o\prime}$ is zero. Combination of eqs 12 and 13 gives

$$\Delta G_{et}^{\ddagger} = \Delta G^{\ddagger}(0)\left(1 + \frac{\Delta G^{o\prime}}{4\Delta G^{\ddagger}(0)}\right)^2 \tag{13}$$

a theoretical expression that can be used to predict rate constants from values of $\Delta G^{o\prime}$ and $\Delta G^{\ddagger}(0)$.[34]

The value of $\Delta G^{o\prime}$ can be determined from the electrochemical potentials for the reactants by including a correction for the work required to bring together the reactants (w_r) and the product anion and cation in the successor complex (w_p).[77] The expression for the free energy of reaction of eq 10 is given in eq 14,

(72) The forward diffusion rate constant can be estimated from the Smoluchowski equation $k_{diff} = 4\pi N_0 Dr$ (see: Moore, J. W.; Pearson, R. G. *Kinetics and Mechanism*, 3rd ed.; Wiley-Interscience: New York, 1981; p 238) where D is the sum of the diffusion coefficients D_1 and D_{ArNO2} calculated to be $D_1 = 8.7 \times 10^{-6}$ cm^2 s^{-1} and $D_{ArNO2} = 1.3 \times 10^{-5}$ cm^2 s^{-1}, respectively (see Kojima, H.; Bard, A. J. *J. Am. Chem. Soc.* **1975**, *97*, 6317), r is the sum of the radii of **1** and $ArNO_2$ and the rest of the terms have their usual meaning. The value of r_{ArNO2} is based on the radius of the aryl ring (3.5 Å). The forward diffusion rate was calculated to be 1.5×10^{10} M^{-1} s^{-1}.

(73) Back diffusion can be estimated from the relationship $k_{-diff} = 3000\ k_{diff}/4\pi r^3 N_0$, (see: Sutin, N.; Brunschwig, B. S. In *Mechanistic Aspects of Inorganic Reactions*; Rorabacher, D. B., Endicott, J. F., Eds.; American Chemical Society: Washington, DC, 1982; Vol. 198, pp 105−125, and Fuoss, R. M. *J. Am. Chem. Soc.* **1958**, *80*, 5059.) where r is the distance between molecules (8.9×10^{-8} cm), and the remaining terms have their usual meaning. The back-diffusion rate constant (k_{-diff}) was calculated to be 8.2×10^9 s^{-1}.

(74) Marcus, R. A. *Annu. Rev. Phys. Chem.* **1964**, *15*, 155.

(75) Marcus, R. A. *J. Chem. Phys.* **1968**, *72*, 891.

(76) Marcus, R. A.; Sutin, N. *Biochim. Biophys. Acta* **1985**, *811*, 265.

(77) Schlesener, C. J.; Amatore, C.; Kochi, J. K. *J. Am. Chem. Soc.* **1984**, *106*, 3567.

$$\Delta G^{o\prime} = F(E^{\circ}_{\mathbf{1}} - E^{\circ}_{\mathrm{ArNO_2}}) + w_p - w_r \qquad (14)$$

where F is the Faraday constant. The standard potential for the oxidization of Ru(dppe)$(CO)_3$ was 0.37 V vs SCE and $E^{\circ}_{\mathrm{ArNO2}}$ is the half-wave reduction potential of the nitroarenes given in Table 5. Both reactants are neutral making w_r negligible. The work term for the interaction between the ion pair (w_p) is based on an electrostatic model for an outer-sphere electron transfer.[78]

On the basis of the value of $\Delta G^{o\prime}$ from eq 14 and appropriate combination of eq 12−13 using a $\Delta G^{\ddagger}(0)$ of 3.5 kcal mol^{-1} [79] one calculates k_{et} to be 2×10^{-12} M^{-1} s^{-1} for the reaction between **1** and 4-chloronitrobenzene where $\Delta G^{\circ\prime}$ was 28 kcal mol^{-1}. The experimental second-order rate constant from Table 5 (1.6×10^{-2} s^{-1} M^{-1}) is 10^{10} times faster than the rate calculated assuming an outer-sphere mechanism. The unfavorable thermodynamics rule out the possibility of an outer-sphere electron-transfer mechanism. A similar mechanistic situation was observed for the substitution of alkyl and aryl halides by nucleophiles where both outer- and inner-sphere electron transfer mechanisms were observed depending on the choice of substrates and reaction conditions.[80] When a measured rate was in agreement with the theoretical rate, based on Marcus theory, an outer-sphere mechanism was favored. When the observed rate was substantially faster an inner-sphere or S_N2 mechanism was favored.[81]

Steric effects have been used as a diagnostic criterion for distinguishing between inner- and outer-sphere electron-transfer mechanisms.[82,83] As can be seen from Figure 7 all nitroarenes (with the exception of substrates **6**, **13**, and **14** and to a lesser extent **4** on Table 5) follow the same correlation. Only nitroarenes bearing bulky substituents or those that had both ortho and meta substituents showed deviation in the rate. This rate retardation provides further evidence that the electron transfer occurs via an inner-sphere mechanism. Lund and Lund found the reaction between sterically hindered alkyl halides and anionic nucleophiles proceeds as an outer-sphere electron-transfer mechanism, whereas less bulky primary and secondary alkyl halides allow closer approach with resulting bond formation upon electron transfer. The rates were 400−2500 times faster than expected for an outer-sphere electron transfer and were consistent with an S_N2 (inner-sphere) mechanism.[84] Similarly Savéant and co-workers found that the substitution mechanism of alkyl halides by Fe(0) and Fe(I) porphyrins or anthracene anions followed these two limiting cases (i.e., outer-sphere vs inner-sphere electron transfer) depending on substrates and reaction temperature. The outer-sphere mechanism exhibited a large $\Delta H^{\ddagger}$ and a near-zero $\Delta S^{\ddagger}$. The inner-sphere (S_N2) mechanism involved low values of $\Delta H^{\ddagger}$ and $\Delta S^{\ddagger}$ values on the order of −20 eu. These observations were rationalized in terms of the transition state of the S_N2 mechanism being more constrained than the outer-sphere mechanism.[85] Direct comparison of our measured $\Delta S^{\ddagger}$ values with Savéant's is not possible due to the difference in the charge type associated with the different reactions.[86] However, the negative value of $\Delta S^{\ddagger}$, measured for the reaction between **1** and unhindered nitroarenes (−33 to −36 eu), is certainly consistent with an inner-sphere electron-transfer mechanism. There was a distinct trend between $\Delta S^{\ddagger}$ and $\Delta H^{\ddagger}$ for the unhindered nitroarenes (Figure 10). The enthalpy of activation for *all* of the nitroarenes decreased as they became more electron deficient. The changes in $\Delta H^{\ddagger}$ were attributed in part to bonding changes between the transition states and the reactants for the different nitroarenes. However, $\Delta S^{\ddagger}$ was observed to increase as the nitroarenes became more electron deficient for *only* the unhindered examples. 2-Trifluoromethylnitrobenzene deviated from the pattern possibly due to an additional unfavorable steric contribution to $\Delta S^{\ddagger}$.

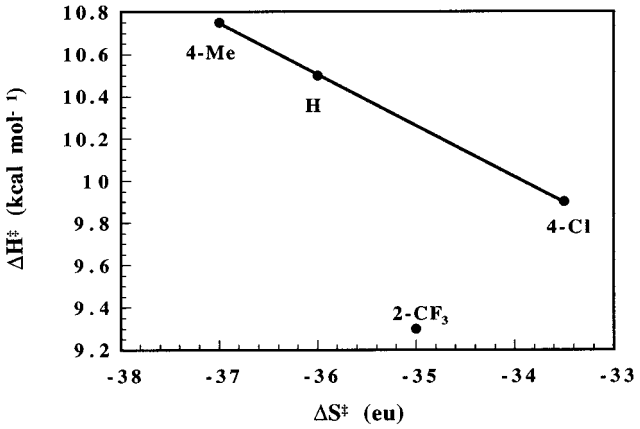

Figure 10. Plot of $\Delta H^{\ddagger}$ vs $\Delta S^{\ddagger}$ for the reaction between Ru(dppe)$(CO)_3$ (**1**) and various nitroarenes in THF.

Inner-Sphere Electron Transfer. The Brønsted slope observed in Figure 7 ($\alpha = 0.59$) is characteristic of mildly endergonic outer-sphere electron transfer.[33] This value of the Brønsted slope is not a sufficient condition for an outer-sphere electron transfer mechanism, since similar relationships have been observed for inner-sphere processes.[87] The relationship between the rates and reduction potentials of the nitroarenes for an inner-sphere electron transfer would resemble outer-sphere behavior if the driving force were shifted by a constant amount; in other words, the variation of the true driving force ($\Delta G^{o\prime}$) parallels that of $-FE^{\circ}_{\mathrm{ArNO2}}$. Cases of inner-sphere electron transfers have been analyzed in terms of a quadratic relationship between log k_{et} and $\Delta G^{o\prime}$ where the unknown driving force for a series of structurally related acceptors with a common donor (or vise versa) differs from the true driving force by a constant amount.[88,89] These types of inner-sphere electron transfers often involve group transfer or group coupling, which can effectively lower the overall driving force.[90] The effect of bonding interactions in an inner-sphere electron transfer would lower the driving force by an inner-sphere work term w_p*. All of the unhindered nitroarenes are assumed to react through a common mechanism, and the work term is assumed to be constant for the series of nitroarene donors. The constancy of the work term is based on the observation that meta and para substituted nitroarenes follow the same correlation (Figure 7). Steric rate retardation was not observed until bulky ortho groups

(78) The work term was calculated from $w_p = -N_o e^2/4\pi\epsilon_o\epsilon r$ where e is electronic charge, ϵ_o is the permittivity of vacuum, and ϵ is the bulk dielectric constant of THF (7.58 from Flick, E. W. *Industrial Solvents Handbook*, 4th ed.; Noyes Data Corporation: Park Ridge, NJ, 1991), and r is the distance between the ion pair (8.9 Å); a value of ∼−5 kcal mol^{-1} was calculated for the work term w_p.

(79) This value of the intrinsic barrier $\Delta G^{\ddagger}(0)$ represents a minimum value, which assumes solvent reorganization only. This minimum value of $\Delta G^{\ddagger}(0)$ would provide the fastest rate possible for the outer-sphere treatment (see ref 34 pp 48−49).

(80) Savéant, J.-M. *Adv. Phys. Org. Chem.* **1990**, *26*, 1.
(81) Lewis, E. S. *J. Am. Chem. Soc.* **1989**, *111*, 7576.
(82) Wong, C. L.; Kochi, J. K. *J. Am. Chem. Soc.* **1979**, *101*, 5593.
(83) Fukuzumi, S.; Wong, C. L.; Kochi, J. K. *J. Am. Chem. Soc.* **1980**, *102*, 2928.
(84) Lund, T.; Lund, H. *Acta Chem. Scand. Ser. B* **1986**, *40*, 470.
(85) Lexa, D.; Saveant., J-M.; Su, K.-B.; Wang, D.-L. *J. Am. Chem. Soc.* **1988**, *110*, 7617.
(86) Halpern, J. *Quart. Rev.* **1961**, *15*, 207.
(87) Cohen, A. O.; Marcus, R. A. *J. Phys. Chem.* **1968**, *72*, 4249.
(88) Lee, K.-W.; Brown, T. L. *J. Am. Chem. Soc.* **1987**, *109*, 3269.
(89) Burke, M. R.; Brown, T. L. *J. Am. Chem. Soc.* **1989**, *111*, 5185.
(90) Pross, A. *Acc. Chem. Res.* **1985**, *18*, 212.

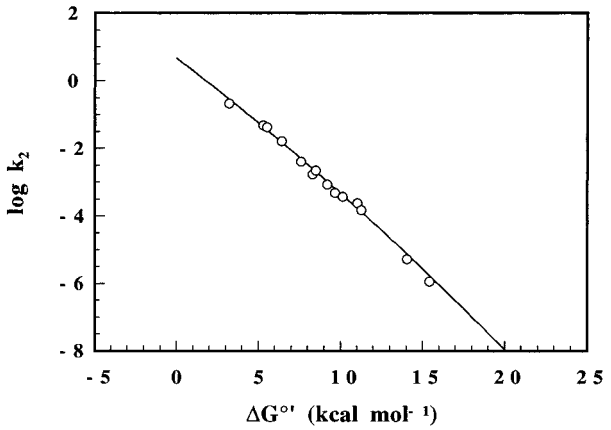

Figure 11. Driving force relationship between log k_2 and $\Delta G^{\circ\prime}$ for the electron-transfer reaction and comparison of the measured rates (points) and calculated rates (line) from eqs 12−14 using $\Delta G^{\ddagger}(0) =$ 14 kcal mol^{-1} and a w_p* value of −26 kcal mol^{-1}.

were used as substituents. We also assume $\Delta G^{\ddagger}(0)$ is constant within the series of nitroarene substrates. These assumptions are reasonable for a homogeneous reaction series such as those between the same reductant and a series of structurally related oxidants that have variable potentials but the same size, shape, electronic structure, and charge.[91,92]

Given the above assumptions the driving force relationship would be amenable to analysis using a linearized form of the quadratic equation (eq 13) to evaluate $\Delta G^{\ddagger}(0)$ and w_p*.[93] These parameters ($\Delta G^{\ddagger}(0) = 14$ and $w_p* = -26$ kcal mol^{-1}) together with eqs 12−14 provide the functional relationship between the experimental rates and driving force (Figure 11).

The values of $\Delta G^{\ddagger}(0)$ and w_p* for the inner-sphere electron-transfer are not quantitatively interpretable in terms of Marcus theory for outer-sphere electron transfer.[94] Qualitatively these parameters are reasonable for an inner-sphere electron-transfer if the reactants and solvent must undergo substantial rearrangement to attain a highly ordered configuration in the transition state, and if there are bonding interactions between the donor and acceptor. A similar mechanism was proposed for the reduction of nitroarenes by α-hydroxymethyl radicals (eq 15)

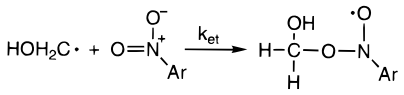

(15)

where a covalent bond yielded a alkoxynitroxyl-type addition product. The transition state for the addition was thought to have pronounced electron-transfer character because the rate increased linearly with the reduction potential of the nitro-

Scheme 2

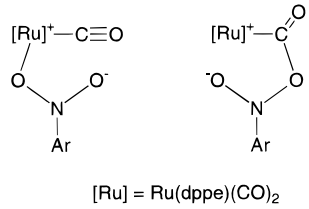

arene.[95,96] By analogy two possible bonding interactions between the donor and the acceptor in the successor complex are given in Scheme 2.

The last step of the mechanism of eq 4 involves deinsertion of CO_2 to form the organometallic product **2**. Cenini and coworkers have observed reversible insertion of CO_2 into the Pt−N bond of the side-bound nitrosoarene in Pt(PhNO)$(PPh_3)_2$.[24,97] The reaction shown in eq 16 is consistant with this related

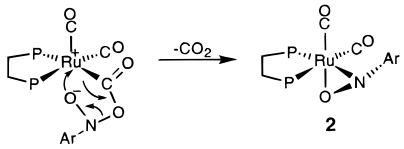

(16)

reaction and the possible structure of the intermediate.

Conclusion

The zerovalent complex Ru(dppe)$(CO)_3$ reacts with nitroarenes to form CO_2 and the structurally characterized η^2-nitrosoarene complex, Ru(dppe)$(CO)_2(\eta_2$-ONAr). The mechanism most consistant with all of the kinetic and thermodynamic data involves oxygen-atom transfer induced by inner-sphere electron transfer.

Acknowledgment. This work was supported by a grant from the National Science Foundation (Grant CHE-9223433). We would like to thank R. A. Marcus, K. R. Mann, and I. Tabakovic for helpful discussions and J. P. Campbell for performing X-ray crystallographic analysis. We also thank a reviewer for valuable comments.

Supporting Information Available: Thermal ellipsoid figure, summary of crystallographic data, atomic positions, thermal parameters, bond distances and angles, and structure factors (43 pages). See any current masthead page for ordering and Internet access instructions.

JA971899W

(91) Sandrini, D.; Gandolfi, M. T.; Maestri, M.; Bolletta, F.; Balzani, V. *Inorg. Chem.* **1984**, *23*, 3017.

(92) Cannon, R. D. *Electron Transfer Reactions*; Butterworths: London, 1980.

(93) A plot of $(\Delta G^{\ddagger})^{1/2}$ (calculated from experimental k_2 values using eq 12) vs $-FE^{\circ}_{ArNO2}/4$ provides a slope (0.226 kcal$^{-1/2}$ mol$^{1/2}$, $r = 0.995$) equal to $(\Delta G^{\ddagger})^{-1/2}$ yielding $\Delta G^{\ddagger}(0) = 14.1 \pm 0.4$ kcal mol^{-1}. From the intercept (2.5 kcal mol^{-1}) a value of w_p* was evaluated (-26 ± 2 kcal mol^{-1}). For an excellent treatment and application of the linearized form of the Marcus equation to an outer-sphere electron transfer, see eq 13 in ref 83 and ref 32 p 1230.

(94) Eberson, L.; Shaik, S. *J. Am. Chem. Soc.* **1990**, *112*, 4489.

(95) Jagannadham, V.; Steenken, S. *J. Am. Chem. Soc.* **1988**, *110*, 2188.

(96) Steenken, S. *Top. Curr. Chem.* **1996**, *177*, 125.

(97) Cenini, S.; Porta, R.; Pizzotti, F.; Crotti, C. *J. Chem. Soc., Dalton Trans.* **1985**, 163.